Journal of Biomedical Optics

SPIEDigitalLibrary.org/jbo

High-contrast subcutaneous vein detection and localization using multispectral imaging

Fengtao Wang
Ali Behrooz
Michael Morris
Ali Adibi

SPIE

High-contrast subcutaneous vein detection and localization using multispectral imaging

Fengtao Wang,[a] Ali Behrooz,[a] Michael Morris,[b] and Ali Adibi[a]
[a]Georgia Institute of Technology, School of Electrical and Computer Engineering, 777 Atlantic Drive, Atlanta, Georgia 30332
[b]Ocean Thin Films Inc., Golden, Colorado 80403

Abstract. Multispectral imaging has shown promise in subcutaneous vein detection and localization in human subjects. While many limitations of single-wavelength methods are addressed in multispectral vein detection methods, their performance is still limited by artifacts arising from background skin reflectance and optimality of postprocessing algorithms. We propose a background removal technique that enhances the contrast and performance of multispectral vein detection. We use images acquired at visible wavelengths as reference for removing skin reflectance background from subcutaneous structures in near-infrared images. Results are validated by experiments on human subjects. [DOI: 10.1117/1.JBO.18.5.050504]

Keywords: multispectral imaging; medical optics instrumentation; subcutaneous imaging; vein detection.

Paper 12806LRR received Dec. 18, 2012; revised manuscript received Apr. 10, 2013; accepted for publication Apr. 11, 2013; published online May 6, 2013.

Subcutaneous vein detection using near-infrared (NIR) imaging has recently become a subject of study.[1–4] Optical absorption of human skin and muscle plummets in the NIR window allowing for light to travel to subcutaneous depths before losing coherence and directionality to diffusion.[5,6] Unlike muscle and skin, blood is a strong absorber of NIR radiation[7] which contrasts the subcutaneous vessels against skin and muscle in NIR imaging. As a result, automatic subcutaneous vein detection has become possible using NIR imaging with extensive application in catheter insertion at health care facilities.[8] It has been shown that multispectral imaging enhances the performance of automatic vein detection as it collects multiple layers of information that are used in image postprocessing software to localize subcutaneous vasculature.[4,8] However, optimal performance of multispectral methods depends on their postprocessing algorithms that require optimal parameter selection and are susceptible to artifacts from nonvein background. Additionally, multispectral methods which use postprocessing software merely detect the subcutaneous vasculature map without retaining other anatomical information. In this letter, we apply a background removal and normalization scheme to multispectral vein imaging that circumvents the limitations of other methods and allows for high-contrast subcutaneous vein detection while extracting nonvein subcutaneous physiological and anatomical structures. At visible wavelengths, images of human limbs mainly entail reflectance from skin, whereas at NIR wavelengths, images are comprised of subcutaneously penetrated light in addition to skin reflectance. To extract the subcutaneous components and remove the skin reflectance, referred to as background herein, from NIR images, we can use the visible images as reference. Visible images taken jointly with NIR images using a multispectral imager are used in a normalized subtraction algorithm to have the background removed from NIR images and bring out the subcutaneous structures. The proposed method is applied to multispectral data obtained by imaging naked arms of human subjects with different skin tone and texture. The output of the algorithm is a fused image that primarily contains subcutaneous components. Multispectral imaging in this work is performed using the Spectrocam™ Multispectral Imaging Camera (Ocean Thin Films, Golden, Colorado). Spectrocam is an imaging system based on a high speed rotating filter wheel coupled to an NIR enhanced CCD camera (a Sony ICX285 sensor) through a Carl Zeiss Distagon 2.8/25 mm ZF-IR lens, as shown in Fig. 1(a). In Spectrocam, multiple wavelengths are multiplexed in the time domain, and as a consequence, the spatial resolution remains un-adulterated. The filter wheel can accept up to eight discrete filters. The camera software separates the images from each filter in real time, and presents the eight spectrally resolved images. In this work, five different filters with the custom-designed spectral bands are utilized, as shown in Fig. 1(b). Narrow-band filters at 546 and 570 nm correspond to the de-oxy and oxy forms of hemoglobin, respectively. The 475 nm broadband filter encompasses the strong absorption bands of melanin, beta-carotene, and hemoglobin. The 615 nm filter covers a region of little absorbance by skin pigments. The 850 nm filter covers the NIR band that includes absorption by lipids but excludes absorption by water.

In the first experiment, Spectrocam was used to perform multispectral imaging on the anterior left forearm of an Asian male under indoor ambient-light environment (without special light source), as shown in Fig. 2. The arm was held still before a dark background. The exposure time under each individual filter is set to 10 ms, and altogether the five spectral images are obtained within 100 ms. Thus, image coregistration from different spectral bands, i.e., motion artifact analysis, is not necessary, especially for still human subjects. As depicted in Fig. 2, it is clear that the unfiltered image and the visible image, shown in Fig. 2(b) and 2(d), have lower vein contrast compared to the NIR image [shown in Fig. 2(c)]. Mathematically, the vein-to-skin (background) contrast ratio, denoted by M, can be defined as below,

$$M = \frac{|U_{\text{vein}} - U_{\text{skin}}|}{(U_{\text{vein}} + U_{\text{skin}})}, \tag{1}$$

where U_{vein} is the average pixel intensity of the vein area, and U_{skin} is the average pixel intensity of intact skin around the veins. The selection of vein and skin areas can be done based on the pixel intensity where four visually selected adjacent skin (high-value) pixels are averaged to obtain U_{skin}, and four visually selected adjacent vein (low-value) pixels are averaged to obtain U_{vein}.

Address all correspondence to: Fengtao Wang, Georgia Institute of Technology, School of Electrical and Computer Engineering, 777 Atlantic Drive, Atlanta, Georgia 30332. Tel: 404 934 0265; E-mail: wangft@yahoo.com

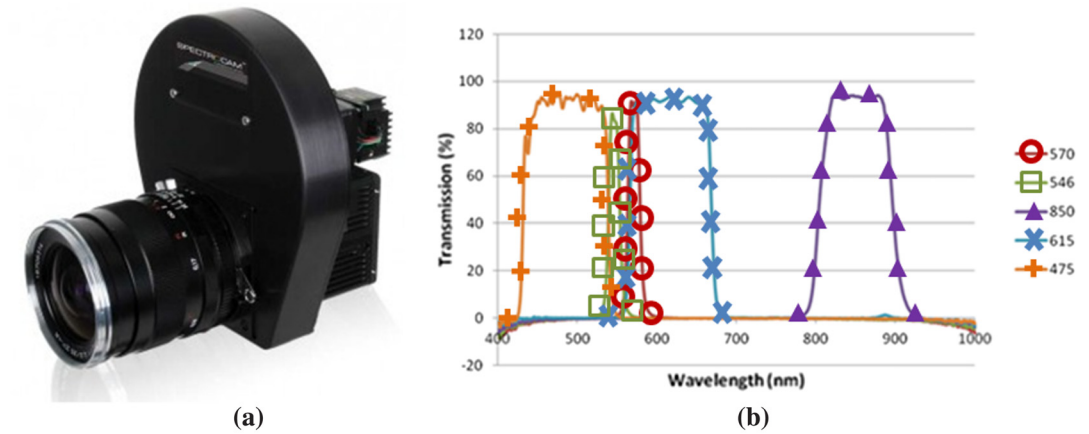

Fig. 1 Spectrocam™ Multispectral Imager. (a) Picture of the imaging system (courtesy of Ocean Thin Films, http://pixelteq.com/product/spectral-cameras). (b) Transmission spectra of filters populating the filter wheel in the Spectrocam: narrow-band 570 nm, narrow-band 546 nm, band-pass 800 to 900 nm, band-pass 560 to 690 nm, and band-pass 410 to 540 nm.

To enhance the contrast of veins against cutaneous background, we use the visible images as reference for skin reflectance and subtract from the NIR image. The reference image must be normalized to match the background component of the NIR image. For the multispectral imaging shown in Fig. 2, we used the proposed normalization/subtraction scheme to arrive at the fused image which, as shown in Fig. 2(e), has a considerably higher visual vein-to-background contrast. The resulting fused image (with the 615 nm image as the reference), as shown in Fig. 2(e), has a contrast ratio M of 0.67, considerably higher than the contrast of 0.037 in the NIR image. Mathematically, the image fusion process can be expressed as below:

$$I_{\text{fused}} = a(I_{850\ \text{nm}} - bI_{\text{ref}}), \tag{2}$$

where I_{ref} represents the reference visible image, $I_{850\ \text{nm}}$ the NIR image, factor a the scalar weight for achieving the appropriate brightness in the fused image, and factor b the normalization weight to enhance vein contrast of the fused image. The optimization of a and b is important for achieving improved visual contrast and brightness in the fused image. In each experiment,

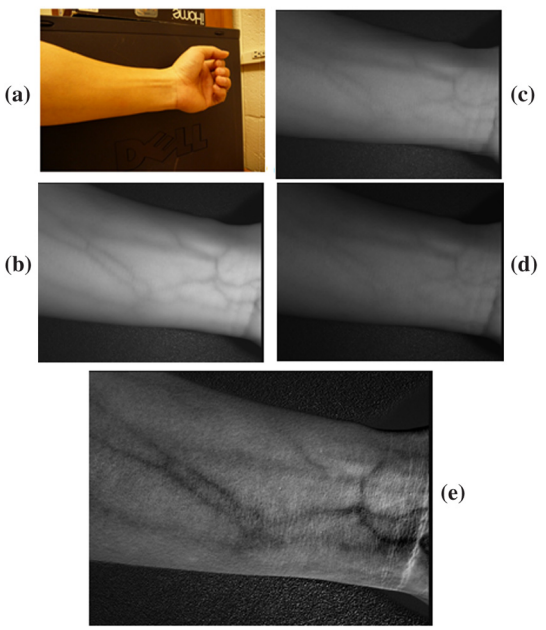

Fig. 2 Multispectral imaging for subcutaneous vein detection. (a) Color image of the anterior left forearm used in multispectral imaging. (b) Unfiltered white light image with $M = 0.01$. (c) near-infrared (NIR) image at 850 nm with $M = 0.033$. (d) Visible image at 615 nm with $M = 0.025$. (e) Fused image of 850 and 615 nm with a contrast ratio of $M = 0.67$, and parameter values of $a = 3$, and $b = 0.64$.

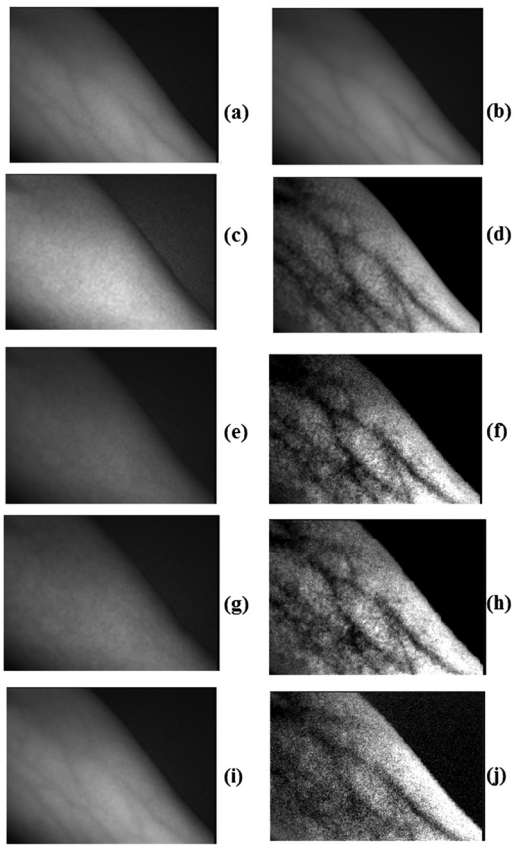

Fig. 3 Multispectral imaging for subcutaneous vein detection. (a) Unfiltered white light image with $M = 0.04$. (b) NIR image at 850 nm with $M = 0.06$. (c) Visible images at 475 nm with $M = 0.01$. (d) Fused images of 850 and 475 nm with $M = 0.61$. (e) Visible image at 546 nm with $M = 0.002$. (f) Fused image of 850 and 546 nm with $M = 0.77$. (g) Visible image at 570 nm with $M = 0.009$. (h) Fused image of 850 and 570 nm with $M = 0.82$. (i) Visible image at 615 nm with $M = 0.04$. (j) Fused images of 850 and 615 nm with $M = 0.47$.

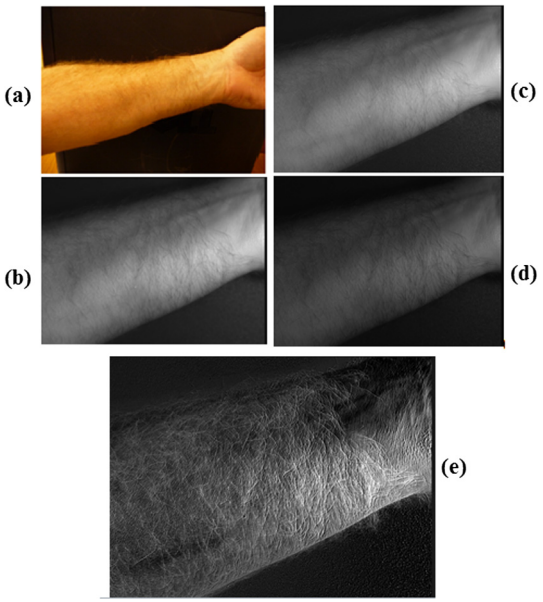

Fig. 4 Multispectral imaging for subcutaneous vein detection on a hairy anterior forearm. (a) Color image of the anterior left forearm used in multispectral imaging. (b) Unfiltered white light image with $M = 0.02$. (c) NIR image at 850 nm with $M = 0.02$. (d) Visible image at 615 nm with $M = 0.01$. (h) Fused image of 850 and 615 nm with a contrast ratio of $M = 0.3$ in the area with lower hair density and parameter values of $a = 2.6$, and $b = 0.37$.

the ballpark optimal values for these parameters are selected automatically by the algorithm. The scaling factor a is simply adjusted to map the highest pixel value in the fused image to the maximum nonsaturated value in the display scale. For the normalization factor b, the ballpark value is selected using the approximate expression below

$$b = (A_{850\,\mathrm{nm}}/A_{\mathrm{vis}})[(M_{\mathrm{fused}} - M_{850\,\mathrm{nm}})/(M_{\mathrm{fused}} - M_{\mathrm{vis}})], \quad (3)$$

where $A_{850\,\mathrm{nm}}$ and A_{vis} are average total intensities of the NIR and reference visible image. For M_{fused}, a desired ballpark value (0.5 in our studies) can be used. Nevertheless, to achieve maximal contrast in the fused images, manual fine-tuning is also performed around the automatically selected optimal values of a and b. In practice, the same procedure can be used for optimization of factors a and b in the clinic where manual adjustment around the automatic ballpark optimal values can be performed by the healthcare specialist using immediate visual feedback from the resulting fused image.

In the second experiment, the proposed technique is applied to the data from multispectral imaging of the anterior forearm of a Caucasian male with very low body hair density. As shown in Fig. 3, a multitude of visible images at 475, 546, 570, and 615 nm are acquired and used as the reference images separately in the background removal technique. The images shown in Fig. 3(d), 3(f), 3(h), and 3(j) are the resulting fused images of the NIR image, shown in Fig. 3(c), and visible images at 475, 546, 570, and 615 nm shown in Fig. 3(c), 3(e), 3(g), and 3(i), respectively. The vein contrast ratios of all four fused images are at least an order of magnitude improved compared to the NIR image. This demonstrates the low sensitivity of the proposed method to the reference visible image wavelength. Our results also show that the performance of the background removal algorithm does not strictly depend on the spectral band selection of the reference visible image as long as it is within a reasonable range (~150 nm) of mid-visible. Also, among the advantages of the proposed technique is that, unlike other multispectral methods, the NIR filter used in the proposed technique does not require sharp narrow-band transmission spectrum. Even with partial overlap of the NIR filter transmission spectrum with visible background spectral window, the contrast of the fused image remains high as the background components are removed from the NIR image and the subcutaneous information not present in the visible images are retained.

Body hair has a strong reflectance glare and can severely impair the vein contrast. To study the effect of excessive density of body hair on the proposed method, anterior forearm of a Caucasian male with a high density of gray hair was imaged by Spectrocam as shown in Fig. 4. The strong glare of the body hair blocks the skin underneath, and the subcutaneous veins have a very low contrast ratio and are almost visually unnoticeable in the NIR image. The fused image, as shown in Fig. 4(e), still provides high vein contrast enhancement for the skin area with moderate hair density, while the subcutaneous veins in high-density hair area remain obstructed. Thus, the proposed technique performs well for a moderate density of body hair as shown in Fig. 4. However, for subjects with excessive density of body hair, the skin must be shaved before using Spectrocam. The cross-polarizer technique is also useful to mitigate hair glare, which shall be addressed in a future study.

In conclusion, we demonstrated that the resulting fused images of three different human subjects with different skin tone all entail clear subcutaneous vasculature maps with contrast enhancement of an order or higher, compared to the NIR images, while retaining the surrounding nonvein physiological structures. The high-contrast and reliable performance of the proposed background removal technique for vein detection and localization in subjects with low to moderate hair density makes it extremely useful for relevant health care applications.

Acknowledgments

This work was supported by the National Institutes of Health (NIH) under the project of "Real-Time Multispectral Early-Stage Pressure Ulcer Detector" (Ref. 9).

References

1. H. D. Zeman et al., "Prototype vein contrast enhancer," *Opt. Eng.* **44**(8), 086401 (2005).
2. V. C. Paquit et al., "Near-infrared imaging and structured light ranging for automatic catheter insertion," *Proc. SPIE* **6141**, 61411T (2006).
3. V. C. Paquit et al., "Combining near-infrared illuminants to optimize venous imaging," *Proc. SPIE* **6509**, 65090H (2007).
4. F. P. Wieringa et al., "Contactless multiple wavelength photoplethysmographic imaging: a first step toward "SpO_2 camera" technology," *Ann. Biomed. Eng.* **33**(8), 1034–1041 (2005).
5. V. V. Tuchin, S. R. Utz, and I. V. Yaroslavsky, "Tissue optics, light distribution and spectroscopy," *Opt. Eng.* **33**(10), 3178–3188 (1994).
6. R. Anderson and J. Parrish, "The optics of human skin," *J. Investig. Dermatol.* **77**(1), 13–19 (1981).
7. S. Wray et al., "Characterization of the near infrared absorption spectra of cytochrome aa_3 and haemoglobin for the non-invasive monitoring of cerebral oxygenation," *Biophys. Acta* **933**(1), 184–192 (1988).
8. V. C. Paquit et al., "3D and multispectral imaging for subcutaneous veins detection," *Opt. Express* **17**(14), 11360–11365 (2009).
9. D. Yi et al., "Real-time multispectral imager for home-based health care," *IEEE Trans. Biomed. Eng.* **58**(3), 736–740 (2011).